

The change of first-flowering date over South Korea projected from downscaled IPCC AR5 simulation: peach and pear

Jina Hur and Joong-Bae Ahn*

Division of Earth Environmental System, Pusan National University, Republic of Korea

ABSTRACT: The variations in the first-flowering date (FFD) of peach (*Prunus persica*) and pear (*Pyrus pyrifolia*) under future climate change in South Korea are investigated using simulations obtained from five models of the fifth Coupled Model Intercomparison Project. For the study, daily temperature simulations with Historical (1986–2005), and Representative Concentration Pathway (RCP) (2071–2090) 4.5 and 8.5 scenarios are statistically downscaled to 50 peach and pear FFD (FFD_{peach} and FFD_{pear} , respectively) observation sites over South Korea. The number of days transformed to standard temperature (DTS) method is selected as the phenological model and applied to simulations for estimating FFD_{peach} and FFD_{pear} over South Korea, due to its superior performance on the target plants and region compared to the growing degree days (GDD) and chill days (CD) methods. In the analysis, mean temperatures for early spring (February to April) over South Korea in 2090 under RCP 4.5 and 8.5 scenarios are expected to have increased by 1.9 and 3.3 K, respectively. Among the early spring months of February to April, February shows the largest temperature increase of 2.1 and 3.7 K for RCP 4.5 and 8.5 scenarios, respectively. The increased temperature during February and March accelerates the plant growth rate and thereby advances FFD_{peach} by 7.0 and 12.7 days and FFD_{pear} by 6.1 and 10.7 days, respectively. These results imply that the present flowering of peach and pear in the middle of April will have advanced to late March or early April by the end of this century.

KEY WORDS AR5 simulations; peach first-flowering date; pear first-flowering date; RCP scenarios; statistical downscaling; temperature projection

Received 1 December 2013; Revised 25 May 2014; Accepted 3 June 2014

1. Introduction

The steep increment of atmospheric greenhouse gases has strengthened the greenhouse warming effect and increased global surface air-temperature by $0.6 \pm 0.2^\circ\text{C}$ in the past century (Intergovernmental Panel on Climate Change (IPCC), 2007). This global warming trend has been more dominant in the winter Northern hemisphere, especially in the mid to high latitudes (Gong and Ho, 2002). For example, the annual mean temperature over South Korea in the mid-latitude has increased by 1.5°C in the last century (Kwon, 2005), which is double the global average.

Global warming causes various scales of climate change and changes in the biosphere through complex interactions between the other subsystems, such as the atmosphere, hydrosphere, cryosphere, and lithosphere. The ecosystem also induces changes in other spheres through complicated interaction and feedback loops. Owing to these ecosystem roles, the effect of climate change on the biosphere has recently been the focus of extensive research in the literature (e.g. Chung *et al.*, 2009, 2011; Jeong *et al.*, 2011; Chmielewski *et al.*, 2012; Jung *et al.*, 2013). In particular, because of changes in phenology, i.e. the seasonal plant activities resulting from environmental variables such as

temperature, moisture, and solar radiation, are sensitive to climate change and easily observed, they are considered a bio-indicator and have recently attracted substantial research interests (Menzel and Fabian, 1999; Menzel and Dose, 2005).

Many studies on phenology (e.g. Guedon and Legave, 2008; Chung *et al.*, 2009; Jeong *et al.*, 2011; Guo *et al.*, 2013) have focused on changes in the first-flowering date (FFD) of deciduous trees in mid- and high-latitudes, as this is strongly affected by the winter and early spring temperature among several climate variables (Menzel and Fabian, 1999; Wielgolaski, 2003). Among deciduous trees, the flowering time for fruit trees is economically important because it is closely related to spring frost damage, pollination, and fruit setting, and is thereby linked to productivity (Cannell and Smith, 1986; Guedon and Legave, 2008). Despite this economic importance, insufficient researches been conducted on regional variation in flowering phenology of fruit trees in association with climate changes (Guo *et al.*, 2013).

Therefore, the aim of this study is to explore the potential effect of future climate changes on the peach (*Prunus persica*) and pear (*Pyrus pyrifolia*) FFDs (FFD_{peach} and FFD_{pear} , respectively) in South Korea. For the study, based on the Historical (1986–2005) and two RCP (2071–2090) simulations of the IPCC AR5 scenario, FFD_{peach} and FFD_{pear} in South Korea are newly estimated using daily gridded temperature from five global climate models.

* Correspondence to: J.-B. Ahn, Department of Atmospheric Sciences, Pusan National University, Pusan 609735, South Korea. E-mail: jbahn@pusan.ac.kr

Table 1. Description of the five CMIP5 coupled models used in this study.

	Institution (country)	CGCM Model name	Model resolution (Lon. × Lat.)	Reference
1	Beijing Climate Center, China Meteorological Administration (China)	BCC-CSM1-1M	320 × 160	Wu <i>et al.</i> (2010)
2	National Center for Atmospheric Research (USA)	CCSM4	288 × 192	Gent <i>et al.</i> (2011)
3	European Earth System Model Consortium (Europe)	EC-EARTH	320 × 160	Hazeleger <i>et al.</i> (2010)
4	Atmosphere and Ocean Research Institute, National Institute for Environmental Studies, and Japan Agency for Marine-Earth Science and Technology (Japan)	MIROC5	256 × 128	Watanabe <i>et al.</i> (2010)
5	Meteorological Research Institute (Japan)	MRI-CGCM3	320 × 160	Mizuta <i>et al.</i> (2012) and Yukimoto <i>et al.</i> (2011)

To minimize the uncertainty of the climate model data, multi-model ensemble (MME) (Krishnamurti *et al.*, 1999; Yun *et al.*, 2003) and mean bias correction methods (Ahn *et al.*, 2012) are applied to the results of the individual model. In addition, three phenological models based on heat or chill accumulation are used and compared for estimating regional FFD_{peach} and FFD_{pear}.

2. Data and method

2.1. Temperature data

For the study, we apply RCP 4.5 and 8.5 climate scenarios, which hypothesize that radiative forcing will be maintained at 4.5 and 8.5 W m⁻² until 2100, respectively (Taylor *et al.*, 2012). The data used are daily Historical (1986–2005) simulation, and RCP (2071–2090) 4.5 and 8.5 gridded temperature data acquired from the fifth Coupled Model Intercomparison Project (CMIP5) archive. Among the many climate models of CMIP5, we chose the five Coupled General Circulation Models (CGCMs) that have a horizontal resolution of 200 km or less, due to South Korea's small area (Hur *et al.*, 2014). Table 1 presents brief information on these five models.

Even though the gridded data produced by the global climate model are very useful in many respects, they are insufficient for dealing with regional climate changes due to the coarse horizontal resolution grid spacing of approximately 100–200 km. Therefore, the global gridded data are statistically downscaled to 50 *in situ* observation sites over South Korea in order to obtain station-scale daily temperature.

As in Hur *et al.* (2014), a hypsometric method, which considers not only inverse distance weighting but also lapse rate correction factor based on elevation difference, is used for statistical downscaling (Dodson and Marks, 1997; Daly *et al.*, 2003). Therefore, the statistically downscaled data reflect the topographical characteristics. The following formulae are used:

$$T_{s_j} = \frac{\sum_{i=1}^n \frac{T_{m_i}}{d_i^2}}{\sum_{i=1}^n \frac{1}{d_i^2}} + \left[Z_{s_j} - \frac{\sum_{i=1}^n \frac{Z_{m_i}}{d_i^2}}{\sum_{i=1}^n \frac{1}{d_i^2}} \right] \Gamma \quad (1)$$

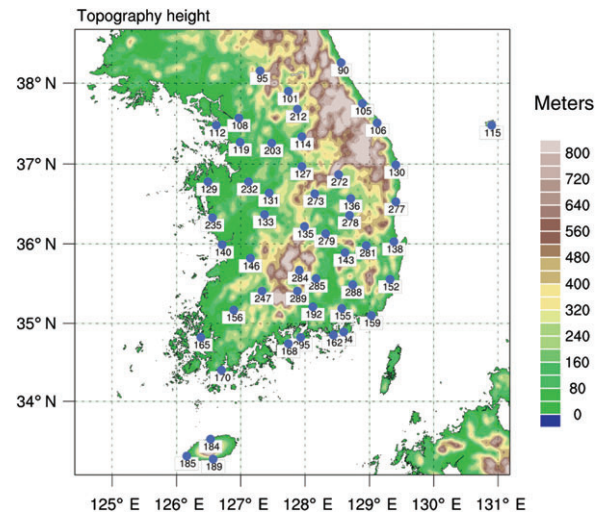


Figure 1. Locations of 50 weather stations (grey dots) observing temperature and FFDs, as well as topography (shaded, m) of South Korea.

$$\Gamma = -1 \times |0.00688 + 0.0015 \cos(0.0172 (\text{Julianday} - 60))| \quad (2)$$

T_{s_j} and Z_{s_j} indicate the daily mean temperature and altitude, respectively, at the j th station among the 50 *in situ* observation sites over South Korea (Figure 1), and Γ is the altitudinal lapse rate derived from empirical experiments (Yun *et al.*, 2000). T_{m_i} and Z_{m_i} are the modelled temperature and altitude, respectively, at the i th grid point in n grid points within the influence radius from the j th observation site. d_i is the distance between the i th grid point and the j th observation site. The radii of influence for BCC-CSM1-1M, CCSM4, EC-EARTH, MIROC5, and MRI-CGCM3 are set as 79, 75, 79, 99, and 79 km, respectively, which are halves of the average grid distance of the individual models (Hur *et al.*, 2014).

To construct three phenological models for estimating FFD_{peach} and FFD_{pear}, daily maximum, minimum, and average temperatures for the three decades from 1981 to 2010 are obtained from the Korean Meteorological Administration (KMA). Daily average temperature data from 1986 to 2005 are reused to remove the mean bias of the climate model and evaluate the simulation skill of

the models. A perturbation method adopted in Ahn *et al.* (2012) is used for minimizing systematic errors. In detail, the modelled and observed data are divided into mean and perturbation parts, and the difference between the two mean parts is eliminated by regarding it as the model's mean bias.

MME is applied to the five CGCMs after removing systematic errors in order to reduce the uncertainty of the individual model (Krishnamurti *et al.*, 1999; Yun *et al.*, 2003). Consequently, this study produced reasonably representative values of each scenario. In performing MME, the simple composite method that has the same weighting factor for all ensemble members is used (Jeong *et al.*, 2012).

2.2. Peach and pear FFD

The FFD_{peach} and FFD_{pear} data from 1981 to 2010 observed by KMA are used to examine the characteristics of current FFD and to evaluate the capability of FFD simulation. FFD is defined as the day when the percentage of each tree's buds that are in full bloom exceeds 20%. Figure 1 shows the distribution of the 50 *in situ* observation sites for temperature and FFDs, as well as the topography of South Korea.

Temperature accumulation models, which are popular due to their rather simple formulae, are adopted as a phenological model for FFD estimation. The following three phenological models are used and concepts of each model are illustrated in Figure 2.

1 The number of days transformed to standard temperature (DTS) (Ono and Konno, 1999): mathematically, DTS is based on a chemical kinetic formula and is the sum of the exponential function of the daily average temperature (Figure 2(a)).

$$\sum_{i=1}^{nday} (\text{daily DTS})_{ij} = \sum_{i=1}^{nday} \left(\exp \left\{ \frac{E_a (T_{ij} - T_s)}{R \times T_{ij} \times T_s} \right\} \right) \quad (3)$$

where T_{ij} is the average temperature, daily DTS_{ij} the daily DTS accumulation on the i th day at the j th station, T_s the standard temperature (271.4 K), R the universal gas constant (8.314 JK⁻¹ mol⁻¹), and E_a the sensitivity of plants to temperature. For the DTS method, three suitable constants are estimated for each fruit tree: (1) D_s , the starting day of calculation (Julian day, JD); (2) E_a , the temperature sensitivity rate (kJ mol⁻¹); and (3) DTS, the accumulated daily DTS from D_s to FFD (days) (Ono and Konno, 1999; Aono and Kazui, 2008; Aono and Saito, 2010; Hur *et al.*, 2014).

2 GDD (Réaumur, 1735; McMaster and Wilhelm, 1997): GDD is a method to estimate the thermal energy requirement for flowering in consideration of the positive relationship between development rate and temperature (Figure 2(a)). It is calculated with the daily maximum and minimum temperatures as follows:

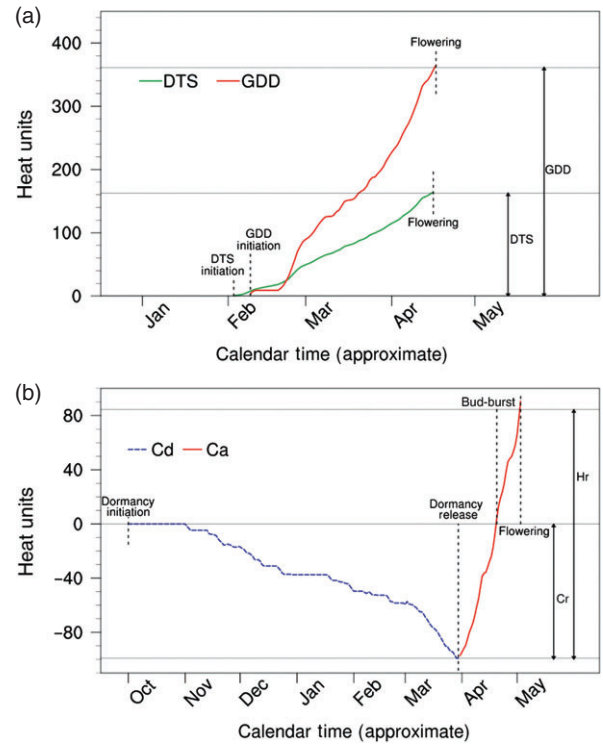


Figure 2. Concepts of the (a) DTS and GDD, (b) CD models estimating flowering date.

$$\sum_{i=1}^{nday} (\text{daily GDD})_{ij} = 0 \quad \text{when } T_m \leq T_{BASE} \quad (4)$$

$$\sum_{i=1}^{nday} (\text{daily GDD})_{ij} = \sum_{i=1}^{nday} (T_m - T_{BASE}) \quad \text{when } T_{BASE} < T_m < T_{UT} \quad (5)$$

$$\sum_{i=1}^{nday} (\text{daily GDD})_{ij} = \sum_{i=1}^{nday} (T_{UT} - T_{BASE}) \quad \text{when } T_m \geq T_{UT} \quad (6)$$

Here,

$$T_m = \left[\left\{ (T_{MAX})_{ij} - (T_{MIN})_{ij} \right\} / 2 \right] \quad (7)$$

$(T_{MAX})_{ij}$, $(T_{MIN})_{ij}$, and daily GDD_{ij} indicate the daily maximum and minimum temperatures, and the daily GDD accumulation on the i th day at the j th station, respectively. T_b and T_{UT} (30 °C) are threshold values of low and high ranks, respectively. Before using the model, three parameters should be set for each plant by users as the DTS case: (1) D_s , the starting day of calculation (JD); (2) T_b , the lower threshold termed the 'base temperature' (°C); and (3) GDD, the accumulated daily GDD from D_s to FFD (GDD) (McMaster and Wilhelm, 1997; Snyder *et al.*, 1999).

3 CD (Cesaraccio *et al.*, 2004; Jung *et al.*, 2005): CD is a two-step model that uses the accumulation of chill

Table 2. Equations to calculate chill days (Cd) and anti-chill days (Ca) for the five cases that relate the maximum (T_x) and minimum (T_n) temperatures to the threshold temperature (T_b), where T is the daily mean temperature (Cesaraccio *et al.*, 2004).

No.	Temperature cases	Chill days (Cd)	Anti-chill days (Ca)
1	$0 \leq T_b \leq T_n \leq T_x$	$Cd = 0$	$Ca = T - T_b$
2	$0 \leq T_n \leq T_b < T_x$	$Cd = -(T - T_n) - \left(\frac{T_x - T_b}{2}\right)$	$Ca = \frac{T_x - T_b}{2}$
3	$0 \leq T_n \leq T_x \leq T_b$	$Cd = -(T - T_n)$	$Ca = 0$
4	$T_n < 0 < T_x \leq T_b$	$Cd = -\left(\frac{T_x}{T_x - T_n}\right)\left(\frac{T_x}{2}\right)$	$Ca = 0$
5	$T_n < 0 < T_b < T_x$	$Cd = -\left(\frac{T_x}{T_x - T_n}\right)\left(\frac{T_x}{2}\right) - \left(\frac{T_x - T_b}{2}\right)$	$Ca = \frac{T_x - T_b}{2}$

days (Cd) to release endodormancy and the accumulation of anti-chill days (Ca) to instigate bloom past the bud-burst date (Figure 2(b)). Negative Cd is accumulated from the onset of dormancy until the chilling requirement (C_r) is attained. If $\sum Cd \leq C_r$, endodormancy is released and positive Ca begins to accumulate towards the heating requirement (H_r). The bud-burst date (BBD) is determined when $\sum Ca + \sum Cd \geq 0$ (i.e. $\sum Ca \geq -1 \times C_r$), whereas FFD occurs when $\sum Ca \geq H_r$. Both Cd and Ca are influenced by a selection of a threshold temperature (T_b) because they are calculated using five equations depending on the daily air temperatures relative to T_b (Table 2).

The onset of dormancy, which determines the starting day of Cd accumulation, can be approximated by a phenological stage such as leaf fall or harvest. However, we assumed a dormancy onset date of October 1, similar to other phenology modelling studies, due to the lack of related data (e.g. Jung *et al.*, 2005; Chung *et al.*, 2009, 2011). In addition to the dormancy onset, three parameters should be properly estimated for each plant: (1) C_r , the chilling requirement (Cd); (2) H_r , the heating requirement (Ca); and (3) T_b , a lower threshold termed the ‘base temperature’ ($^{\circ}C$).

By applying combinations of the three constants to temperature data observed for 30 years from 1981 to 2010, the most suitable parameter combination for each model is chosen and the model performance evaluated. To project future FFD changes, the model with the best estimation ability is selected and then applied to the simulated station-scale temperature.

3. Results and discussions

3.1. Performance evaluation of the FFD estimation models

First, the three appropriate parameters for DTS, GDD, and CD models are determined to estimate FFD_{peach} and FFD_{pear} in South Korea. Considering the average FFD_{peach} (JD: 98.5) and FFD_{pear} (JD: 102.3) for 30 years, we set D_s at JD 18–40 for peach and JD 22–44 for pear with 2-day intervals in the DTS and GDD models. To identify the most suitable parameters in DTS, we set E_a from 40–76 $kJmol^{-1}$ at 4 $kJmol^{-1}$ intervals, and calculate DTS with 120 combinations [12 (the number of D_s) \times 10 (the

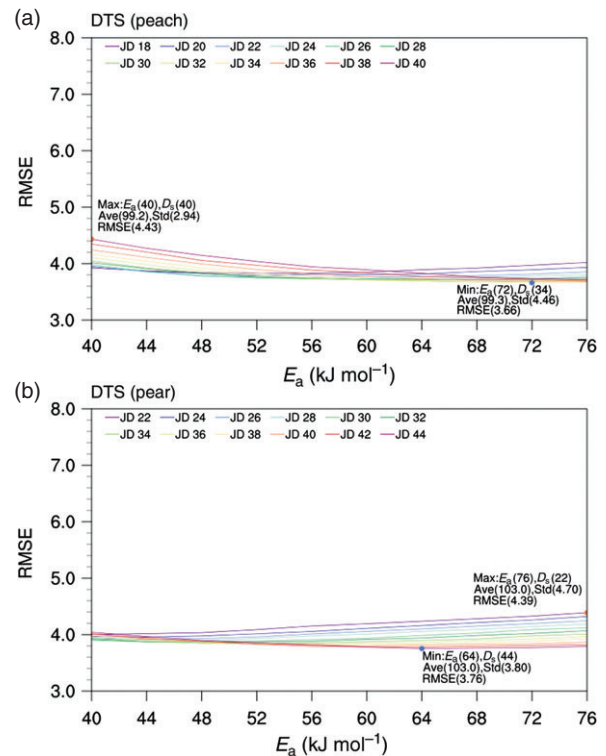


Figure 3. Changes in root mean square error (RMSE) of FFDs according to the variation of parameters in the DTS model using observed temperature and FFD data from 1981 to 2010.

number of E_a]). In the case of GDD, T_b is set from 0 to 10 $^{\circ}C$ at 1 $^{\circ}C$ intervals, giving a total of 132 combinations [12 (the number of D_s) \times 11 (the number of T_b)]. Then, FFD_{peach} and FFD_{pear} are estimated using each combination and the corresponding DTS and GDD. The combination with the lowest root mean square error (RMSE) between the observed and estimated FFDs is decided as the most appropriate (Snyder *et al.*, 1999; Cesaraccio *et al.*, 2004; Aono and Kazui, 2008; Hur *et al.*, 2014). According to the result, DTS has the lowest RMSE for peach and pear in South Korea when E_a is 72 and 64 $kJmol^{-1}$ and D_s is JD 34 and 44, respectively (Figure 3). GDD has the lowest RMSE when T_b is 0 $^{\circ}C$ and D_s is JD 40 for peach and JD 44 for pear (Fig. 4). The estimated D_s in the study is early- to mid- February for both trees. According to the physiological interpretation of Ono and Konno (1999), this period roughly corresponds to that of endodormancy release.

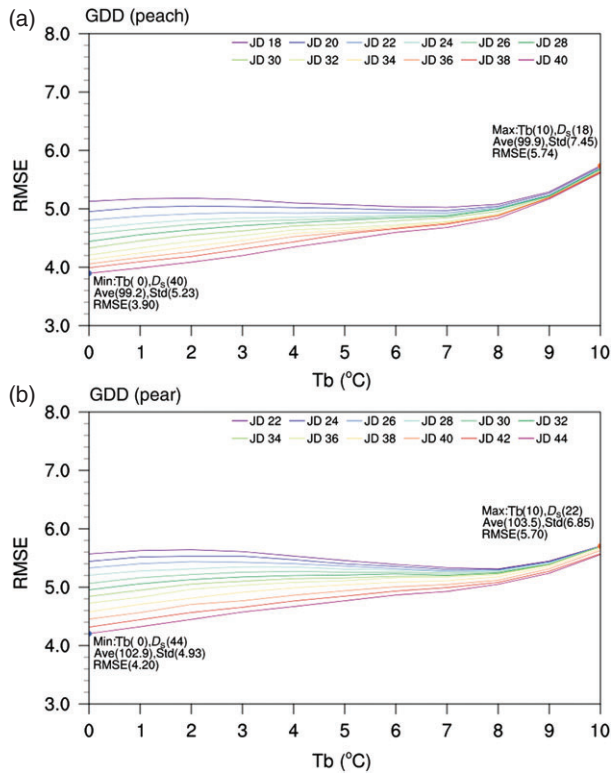


Figure 4. Changes in root mean square error (RMSE) of FFDs according to the variation of parameters in the GDD model using observed temperature and FFD data from 1981 to 2010.

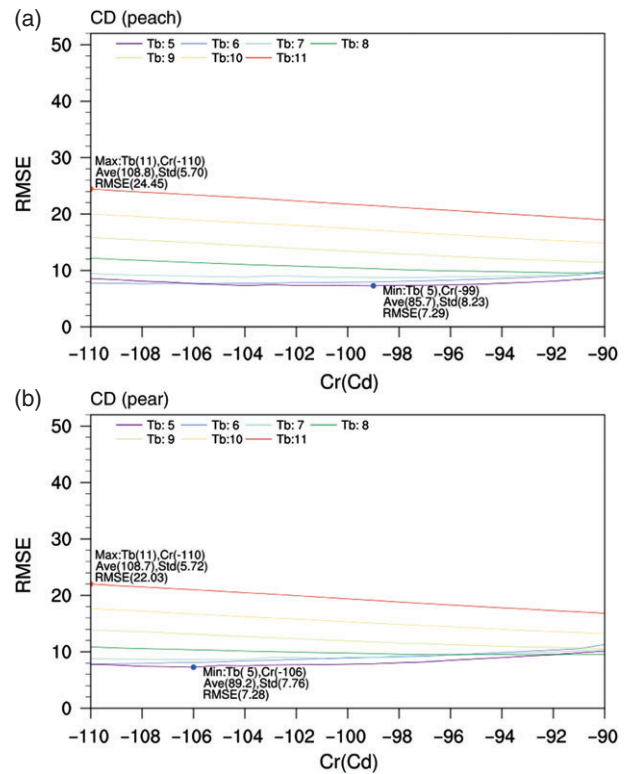


Figure 5. Changes in root mean square error (RMSE) of BBDs according to the variation of parameters in the CD model using observed temperature and BBD data from 1981 to 2010.

A two-step procedure is used to estimate the optimal parameters of the CD model. The parameter optimization method is basically the same as the one described in Jung *et al.* (2005) who suggest flowering model by extending bud-burst model of Cesaraccio *et al.* (2004). First, the optimal C_r and T_b are selected using BBD data by considering that BBD occurs when $\sum Ca \geq -1 \times C_r$. BBD is defined when over 20% of each tree's floral buds burst open. The BBD data used in this study are taken from KMA observations, which have the same observation sites and period as those of FFD. C_r is set from -90 to -110 Cd at -1 Cd intervals. T_b is set from 5 to 11 °C at 1 °C intervals by taking failure rates on bud-burst open into consideration. In detail, the failure rate on bud-burst open is over 20% when T_b is below 4 °C or above 12 °C. Therefore, BBD is estimated with 147 treatments [21 (the number of C_r) \times 7 (the number of T_b)]. Then, RMSE is calculated for each combination in the estimation of BBD for 30 years. The best combination of C_r and T_b is selected as the one that affords the smallest RMSE between the observed and estimated BBDs. According to the result, CD has the lowest RMSE in South Korea when C_r are -99 and -106 Cd and T_b is 5 °C for peach and pear, respectively (Figure 5). In the second step, the most suitable H_r is determined using C_r (-99 and -106 Cd for peach and pear, respectively) and T_b (5 °C) selected in step 1. When we taking into account that FFD occurs when $\sum Ca \geq H_r$, annual H_r is calculated by accumulating Ca from endodormancy release (the day when $\sum Cd \leq C_r$) till FFD observed at each year. The

average H_r for 30 years is selected as the optimal parameter. Consequently, 183.3 and 199.4 Ca are selected as H_r for peach and pear, respectively. Table 3 shows three parameters for each model and species that were determined by RMSE analysis to be the most suitable study values.

Model performance is evaluated based not only on quantitative estimation such as temporal correlation coefficient (TCC) and RMSE but also on categorical estimation such as Hit Rate (HR) and Heidke Skill Score (HSS). Evaluation is performed at each station and averaged over 50 stations. HR and HSS are calculated using three categories based on one standard deviation (6 days) of FFD_{peach} and

Table 3. Three parameters for DTS, GDD, and CD models that were determined to be the most suitable study values by the analysis of root mean square errors (RMSE).

		Peach	Pear
DTS	D_s (JD)	34	44
	E_a (kJ/mol)	72	64
	DTS (days)	162.7	145.8
GDD	D_s (JD)	40	44
	T_b (°C)	0	0
CD	GDD (GDD)	361.1	395.5
	T_b (°C)	5	5
	C_r (Cd)	-99	-106
	H_r (Ca)	183.3	199.4

Table 4. Average and skill scores of FFDs derived from DTS, GDD, and CD models using observation during 30 years from 1981 to 2010.

		Observation	DTS	GDD	CD
Peach	Average (JD)	98.5	99.3	99.2	100.7
	RMSE (day)	–	3.66	3.90	5.08
	TCC	–	0.72**	0.71**	0.67**
	HR	–	0.73	0.71	0.70
	HSS	–	0.58	0.54	0.52
Pear	Average (JD)	102.3	103.0	102.9	104.5
	RMSE (day)	–	3.76	4.20	5.18
	TCC	–	0.69**	0.68**	0.59**
	HR	–	0.75	0.72	0.67
	HSS	–	0.62	0.56	0.47

**99% confidence level (± 0.46).

FFD_{pear}: below normal (< -6 day), normal (≥ -6 day and ≤ 6 day) and above normal (> 6 day). Table 4 shows the skill scores and average of FFD_{peach} and FFD_{pear} derived from the DTS, GDD, and CD models using observed temperature for 30 years from 1981 to 2010. The observed average FFD_{peach} and FFD_{pear} are 98.5 and 102.3 days, respectively, indicating that peach and pear generally flower in early- or mid-April in South Korea. Average FFD_{peach} and FFD_{pear} estimated by DTS, GDD, and CD are similar to the observation with relatively slight margins of about 2 days. DTS has better skill than GDD and CD in terms of RMSE and TCC, although even GDD and CD have sufficiently low RMSE and high TCC with 99% confidence level for FFD_{peach}. As for the two categorical estimation concerns, DTS shows better estimation ability for peach in South Korea because HR and HSS are closer to 1 compared to the other models. For pear, DTS also shows lower RMSE and higher TCC, HR, and HSS. These results confirm the validity of these three methods for estimating FFD_{peach} and FFD_{pear} in South Korea. In particular, FFD derived from DTS is more similar to the observed data than that derived from GDD and CD according to various evaluations. This agrees with the claims of Aono and Kazui (2008) that DTS is more appropriate than GDD for estimating cherry FFD in Japan. Even though the CD model is a more mechanistic approach than DTS and GDD, its estimation ability for FFD_{peach} and FFD_{pear} in South Korea is lower than that of the others due to uncertainties arising from many factors such as the dormancy onset and release, and bud-burst. Therefore, the rather simple DTS is chosen in this study as the phenological model and is applied to the simulated temperature in order to estimate future FFD changes over South Korea.

3.2. Change of FFD_{peach} and FFD_{pear}

To select a target season and to determine the temperature dependency of FFD, the relationship between temperature and the FFD of each fruit tree is examined using the 30-year observation data. Figure 6 shows the average TCC between the 10-day average temperature from January to April and FFD_{peach} and FFD_{pear}. This period was selected as many plants are dormant and start flowering in South Korea (Jeong *et al.*, 2011). There is a statistically

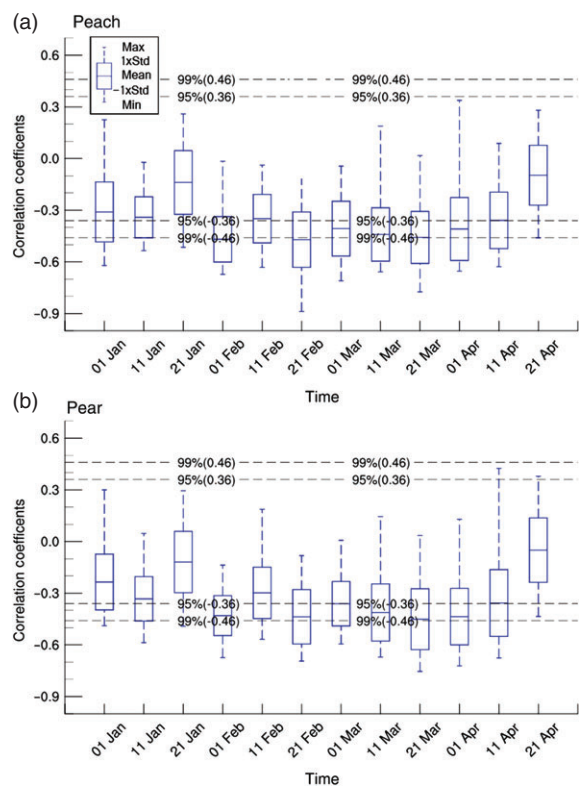


Figure 6. Correlation coefficients between 10-day mean temperatures and FFDs for 1981–2010 averaged over 50 stations. Vertical boxes and bars represent one standard deviation and maximum and minimum values among the 50 stations, respectively. Dashed lines indicate the 99 and 95% confidence levels of correlation coefficient.

significant ($p < 0.05$) negative correlation between the temperatures of February to April and FFD_{peach} and FFD_{pear}. This strong temperature dependency of the two FFD values during these 3 months, which we term early spring, led us to investigate the changes in early spring temperature.

Changes in early spring temperature in association with global warming and the corresponding DTS variations of each month are estimated using simulated daily temperature. Table 5 shows the monthly average temperature and accumulated DTS derived from observation (1986–2005), Historical (1986–2005) simulation, and

Table 5. Accumulated DTS and mean temperature for three months from February to April at 50 stations over South Korea.

			February	March	April
Accumulated DTS (days)	Peach	Observation	44	80	39
		Historical	42	80	44
		RCP 4.5	52	92	21
	Pear	RCP 8.5	62	96	8
		Observation	27	73	46
		Historical	25	72	50
		RCP 4.5	31	85	32
Mean temperature (K)	RCP 8.5	36	95	18	
	Observation	274.9	279.5	285.7	
	Historical	274.9	279.5	285.7	
	RCP 4.5	277.0	281.3	287.4	
	RCP 8.5	278.6	282.7	288.7	

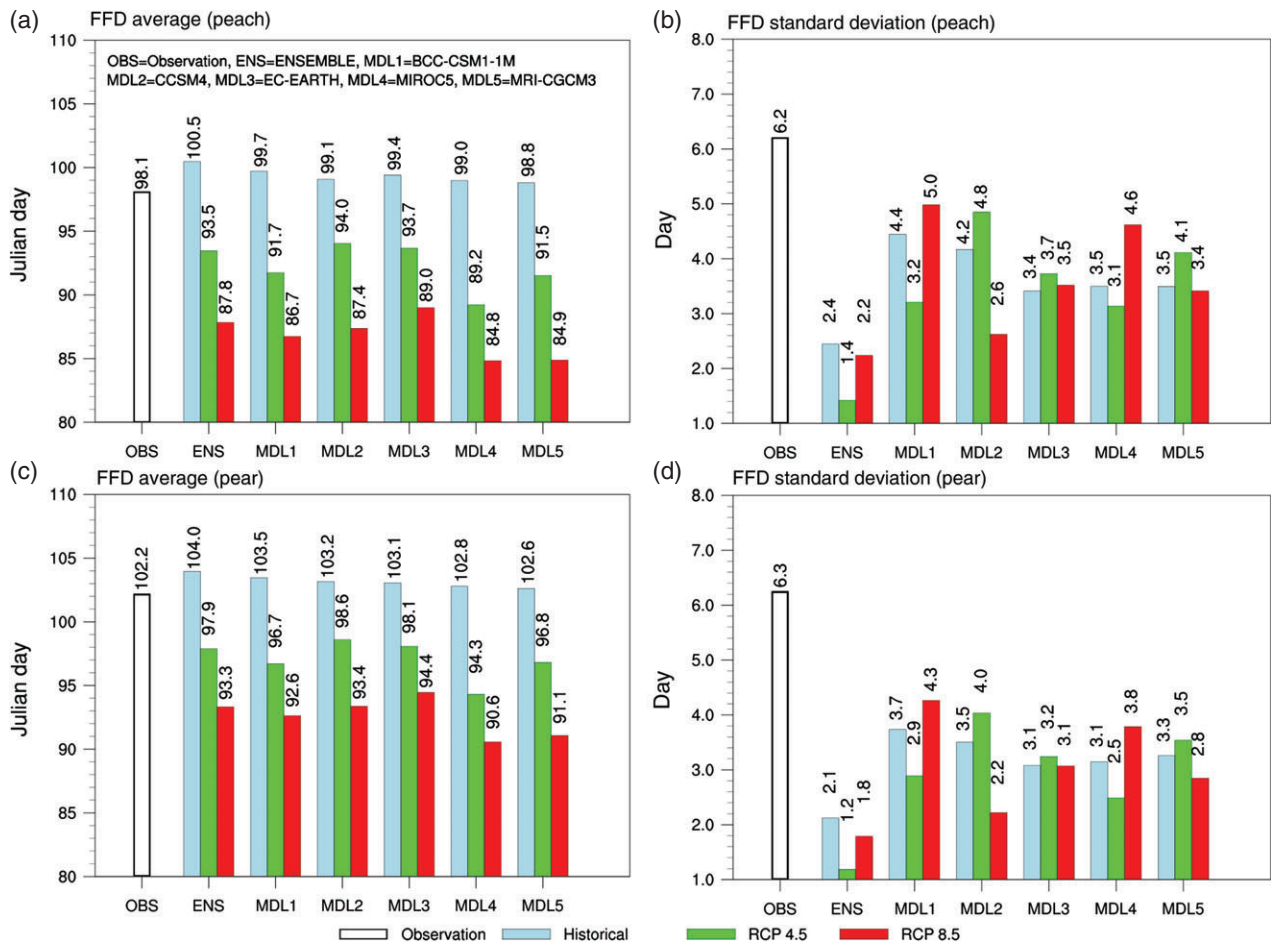


Figure 7. Average FFDs (left, Julian day) and standard deviations of FFDs (right, day) derived from observation (for 1986–2005, white), and Historical (for 1986–2005, light grey), RCP 4.5 (for 2071–2090, dark grey), and RCP 8.5 (for 2071–2090, black) simulations.

RCP (2071–2090) 4.5 and 8.5 simulations. In climatology, the monthly average temperature increases by 4.6 and 10.8 K from 274.9 K in February to 279.5 and 285.7 K in March and April, respectively. By 2090, the average temperatures over South Korea simulated under the RCP 4.5 (RCP 8.5) scenario are anticipated to increase by about 2.1 K (3.7 K) in February, 1.8 K (3.2 K) in March, and 1.7 K (3.0 K) in April. As a result, the temperature increase is higher under the RCP 8.5 scenario than under RCP 4.5

and higher in February than in April. This is attributed to the snow albedo feedback mentioned in Ohashi and Tanaka (2010) and Im and Ahn (2011). According to their study analysis, melted snow in high elevation causes decreased albedo and increased insolation, which means that the temperature changes in winter (December to February, DJF) can be larger than those in other seasons in South Korea. This result agrees with the analysis of Im *et al.* (2008), who found that winter (DJF) exhibits a larger temperature

change than does summer (June to August, JJA) under the SRES B2 scenario.

In the observation and Historical simulations, accumulated monthly DTS is the highest in March. The high level of DTS accumulation in February and March implies that the daily average temperature for the period is warm enough for plants to grow after D_s (JD: 40 and 44 for peach and pear, respectively), which roughly corresponds to the date of endodormancy release (Ono and Konno, 1999). Moreover, the DTS accumulation in April is smaller than that in February and March, despite the higher average temperature, because sufficient DTS is accumulated during the preceding 2 months, leaving only a small amount of accumulable DTS remaining. This means that the temperature of the two preceding months has a greater effect on flowering, although the average temperature in the period is lower than that in April. The DTS accumulation derived from the RCP simulations tends to decrease in April but to increase in February and March. Accumulated DTS for peach (pear) tree is expected to increase by about 10 and 20 days (6 and 11 days) in February, and by 12 and 16 days (13 and 23 days) in March, compared to the Historical simulation under RCP 4.5 and 8.5 scenarios, respectively. On the other hand, it is expected to decrease by about 23 and 36 days (18 and 32 days) in April. Because the total DTS amount is fixed, the increased temperature and DTS accumulation in February and March lead to decreased DTS accumulation in April. In other words, as early spring temperature rises under global warming, FFD_{peach} and FFD_{pear} will become increasingly affected by February and March temperature but less affected by April temperature. This means that the floral development will be accelerated in the two preceding months, in agreement with Chung *et al.* (2011).

Figure 7 shows the average and standard deviation of FFD_{peach} and FFD_{pear} derived from observation and climate models. Observed current FFD_{peach} and FFD_{pear} are JD 98.1 and 102.2, respectively, on average. This indicates that these two trees mostly start flowering in mid-April. FFD_{peach} moves forward by about 7.0 and 12.7 days compared to the Historical simulation by 2090 under RCP 4.5 and 8.5 scenarios, respectively, so that peach is expected to flower in late March or early April in 2090. Considering that the FFD_{peach} trend observed from 1954 to 2004 is $-2.46 \text{ days } ^\circ\text{C}^{-1}$ (Jeong *et al.*, 2011), the average advances (-3.68 and $-3.84 \text{ days } ^\circ\text{C}^{-1}$) in the RCP 4.5 and 8.5 simulations are -1.22 and $-1.38 \text{ days } ^\circ\text{C}^{-1}$ higher, respectively, than the observation. As in the case of peach, FFD_{pear} is expected to advance by 6.1 and 10.7 days in 2090 with a negative trend towards temperature of -3.21 and $-3.24 \text{ days } ^\circ\text{C}^{-1}$ under RCP 4.5 and 8.5 scenarios, respectively. Assuming steady advances, the average annual FFD advances in the RCP 4.5 and 8.5 simulations will be 0.08 and $0.15 \text{ days year}^{-1}$ for peach and 0.07 and $0.13 \text{ days year}^{-1}$ for pear, respectively. This result shows that the increase in February and March temperature will accelerate the growing speed of peach and pear trees and advance the flowering date.

Kim *et al.* (2013) determined that the average FFD of forsythia, azalea, and cherry blossom will advance by 25 days from 2071 to 2100 under RCP 8.5 scenario, which is more than 10 days faster than the advance estimated in this study. Even with due regard to the possible discrepancy in various factors such as climate data, phenological model, and tree type, this is a large difference. Considering that those plants flower earlier than peach and pear, the difference can be attributed to the insistence of Roetzer *et al.* (2000) that early-flowering species are more variable in flowering time than late-blooming species.

The observed FFD_{peach} and FFD_{pear} have an average standard deviation of 6.2 and 6.3 days, respectively. All simulations, including MME results, have lower variations than that of observation. This is a general characteristic of climate prediction models that underestimate the fluctuations of variables such as temperature (Ines and Hansen, 2006; Hur *et al.*, 2014). Moreover, the change in the standard deviations of FFDs did not exhibit any relationship with global warming in this study.

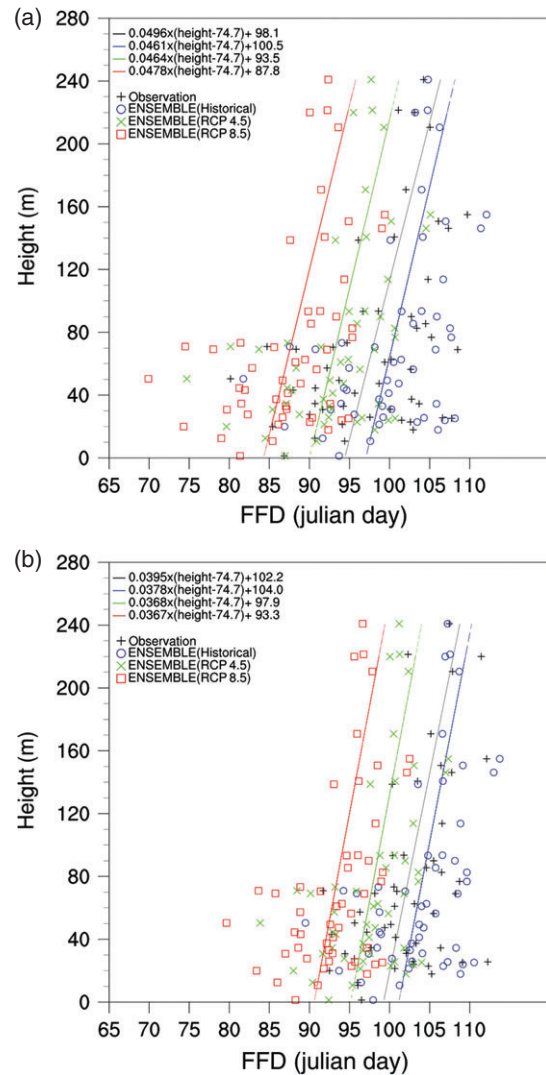


Figure 8. Scatter plots of the altitude of 50 stations against peach (a) and pear (b) first-flowering date (FFD) at the corresponding locations.

The altitude dependency of FFD_{peach} and FFD_{pear} changes is also investigated (Figure 8). FFD_{peach} and FFD_{pear} at high altitude are delayed compared to those at low altitude due to lower daily average temperature. The temperature change rate with the altitude of observation is -1.17 , -1.16 , -1.13 , -1.11 °C/100 m in Historical, RCP 4.5, and RCP 8.5 simulations, respectively, indicating that the high altitude temperature increases slightly more than the low altitude temperature under global warming. According to Student's *t*-test, the variation of the temperature change rate with altitude under RCP 4.5 and 8.5 scenarios is statistically significant at 82 and 65% confidence levels, respectively. This characteristic of temperature change with altitude is in agreement with the results of Im and Ahn (2011), who attributed it to the snow-albedo feedback mechanism. This characteristic infers that the FFD delay with increasing altitude in RCP 4.5 and 8.5 simulations will be reduced compared to the Historical simulation. However, unlike our inference, the

slopes of FFD_{peach} in the two RCP simulations are steeper than that in the Historical simulation in the peach case. While the FFD_{peach} change with altitude occurs more steeply in the future projection, the slope of FFD_{pear} with elevation shows a decrease of 0.10 and 0.11 day/100 m in RCP 4.5 and 8.5 simulations, respectively, compared to the Historical simulation (Figure 8). Hur *et al.* (2014) presented similar results and gave two explanations. Firstly, all stations used for the analysis are located under 280 m elevation, which explains the limit in clearly explaining the altitude dependency of FFD change. Secondly, flowering is affected not only by temperature but also by other environmental variables such as day-length, moisture, and solar radiation. Therefore, FFD change will not show a linear correlation with temperature variation (Diekmann, 1996; Tyler, 2001; Yeang, 2007).

The spatial distribution of FFD_{peach} derived from observation and simulations is shown in Figure 9. Observed

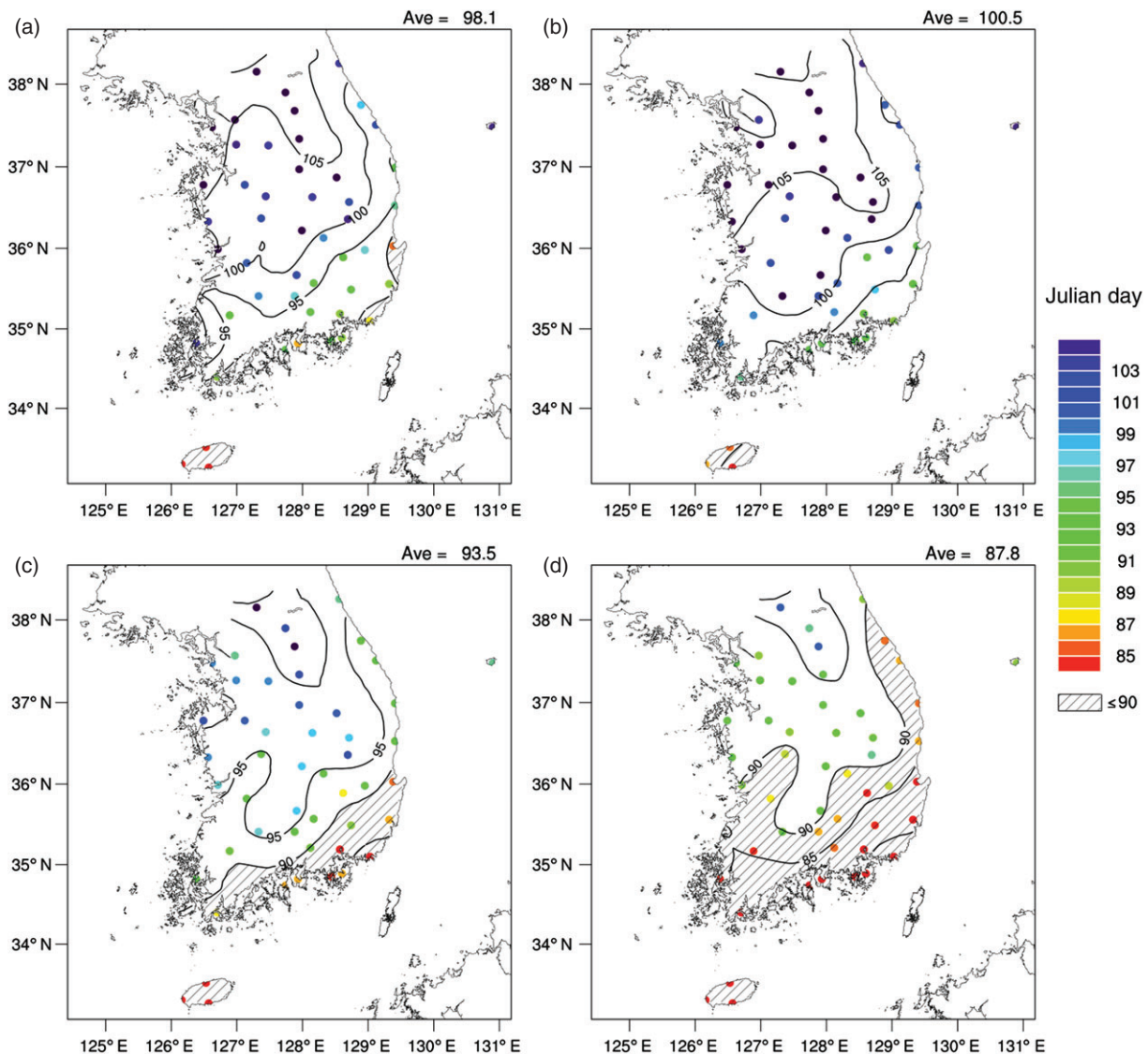


Figure 9. Spatial distribution of FFD_{peach} derived from observation (for 1986–2005, (a), and Historical (for 1986–2005, (b), RCP 4.5 (for 2071–2090, (c), and RCP 8.5 (for 2071–2090, (d) simulations for the flowering period (February–April). Unit is Julian day.

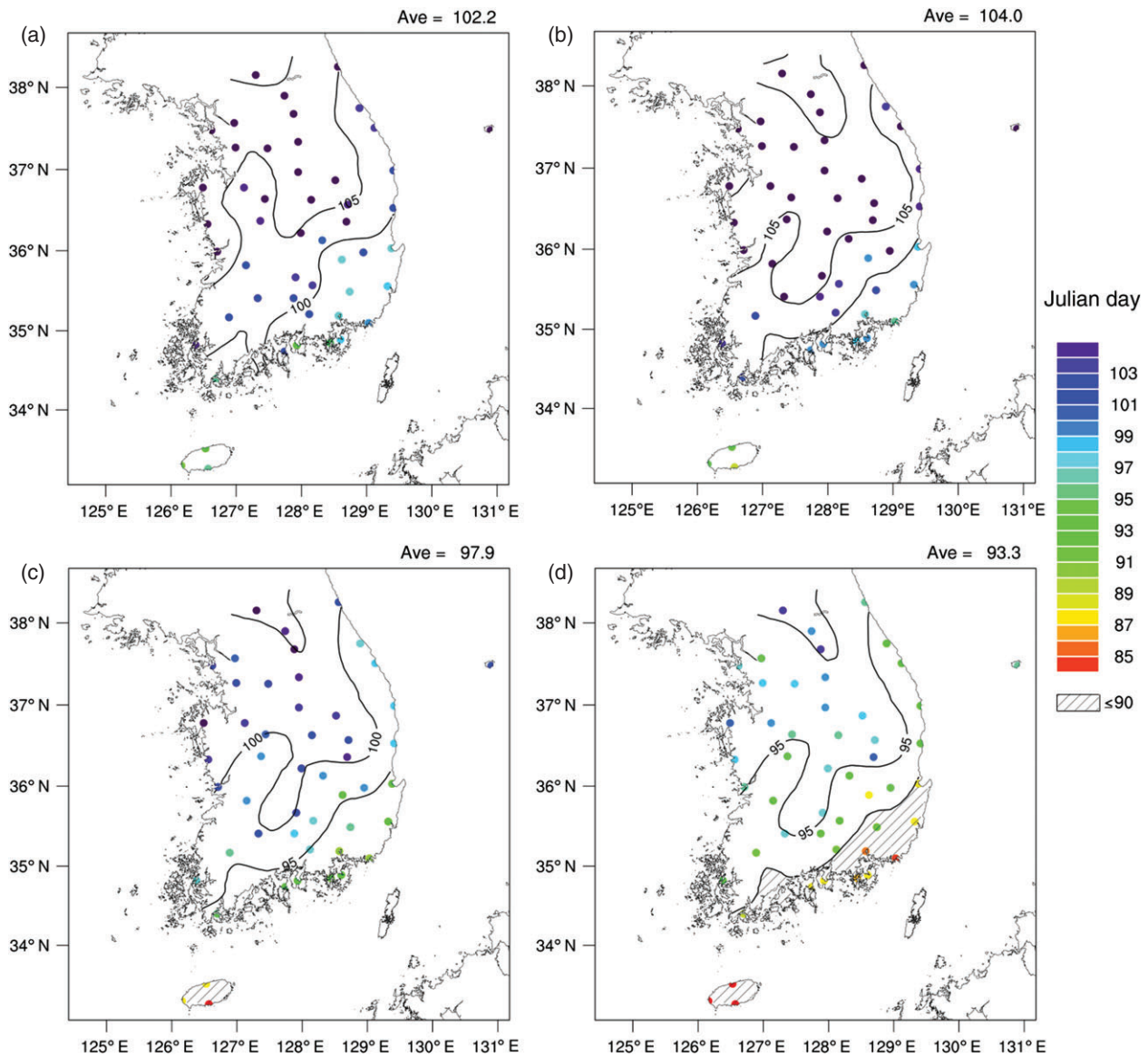


Figure 10. Spatial distribution of FFD_{pear} derived from observation (for 1986–2005, a), and Historical (for 1986–2005, b), RCP 4.5 (for 2071–2090, c), and RCP 8.5 (for 2071–2090, d) simulations for the flowering period (February–April). Unit is Julian day.

FFD_{peach} on average is JD 98.1, which reflects the topographical signal. FFD_{peach} is earlier at low altitude and in flatland than at high altitude and in mountainous regions. The Historical simulation successfully simulates the spatial pattern and general characteristics of the observation in qualitative terms but gives an estimated FFD_{peach} that is 2.4 days later than observation in quantitative terms. The JD 90 line is located around 33.5°N in the observation and Historical simulation at 126.5°E (the location of Jeju island off the southern tip of the Korean peninsula), indicating that peach flowers in March over the region. The areas with values lower than JD 90 account for 3.8 and 1.8% of the land area of South Korea in the observation and Historical simulation, respectively. FFD_{peach} under RCP 4.5 and 8.5 scenarios is uniformly advanced over all stations, irrespective of the altitude, compared to that of the Historical simulation (Figure 8), while maintaining a topographical

effect on FFD. The JD 90 line moves northward by 1°N and 2.5°N to 34.5°N and 36.0°N at 126.5°E under RCP 4.5 and 8.5 scenarios, respectively, 85 years later. This indicates that the two RCP simulations have a northward moving speed of approximately 0.01 and 0.03°N year⁻¹, respectively. Therefore, areas with values lower than JD 90 are increased to about 15.6 and 45.5% in RCP 4.5 and 8.5 simulations, respectively.

The spatial distribution of FFD_{pear} derived from observation and simulations is shown in Figure 10. Observed FFD_{pear} on average is JD 102.2, which well reflects the topographical signal, as in the peach case. FFD_{pear} in the Historical simulation is JD 104.0, which is later on average than in the observation, indicating that the climate models underestimate the flowering time in general. In qualitative terms, however, the model captures the spatial pattern of observation in that FFD_{pear} appears relatively early in the

southern and eastern coasts. FFD_{pear} derived from RCP 4.5 and 8.5 simulations advances by 6.1 and 10.7 days, respectively, in all stations in 2090. Quantitative analysis reveals that the JD 90 line, which is not shown in the observation and Historical simulation, appears at 33.5°N and 34.5°N at 126.5°E under RCP 4.5 and 8.5 scenarios, respectively. The areas with values lower than JD 90 are increased from 0 to about 1.8 and 12.8% of the land area of South Korea in RCP 4.5 and 8.5 simulations, respectively. This implies that pear is expected to start flowering in late March by the end of this century, compared to mid-April on average these days.

4. Summary and conclusion

In this study, regional early spring temperature changes and accompanying FFD_{peach} and FFD_{pear} variations over South Korea in association with global warming were estimated using the observation (1986–2005), Historical (1986–2005) simulation, and RCP (2071–2090) 4.5 and 8.5 simulations of the IPCC AR5 scenario. For the study, global-scale gridded data were statistically downscaled into *in situ* observation stations in South Korea. The systematic bias of each model was eliminated and MME was performed using five CGCM outputs in order to obtain reliable estimation. The DTS phenological model was applied to the downscaled temperature data due to its better performance on the target plants and region compared to GDD and CD in terms of various quantitative and categorical estimations. Temperature for the three spring months from February to April was used in the analysis because it was correlated with FFD_{peach} and FFD_{pear} at the 95% confidence level.

By 2090, early spring temperature in RCP 4.5 and 8.5 simulations was increased by 1.9 and 3.3 K compared to that in the Historical simulation, respectively. The temperature change was the highest in February, followed by that in March and April. This increasing mean temperature in February and March increased the DTS accumulation during the period, which implies that the increased temperature accelerated the growth rate of peach and pear and thereby advanced FFD_{peach} by 7.0 and 12.7 days and FFD_{pear} by 6.1 and 10.7 days under RCP 4.5 and 8.5 scenarios, corresponding to advancement trends of 0.08 and 0.15 days year⁻¹ for peach and 0.07 and 0.13 days year⁻¹ for pear, respectively. Therefore, the current mid-April FFD_{peach} and FFD_{pear} over South Korea are expected to advance to late March or early April by the end of this century.

This study only examined the effect of early spring temperature on FFD, and not that of other season temperatures or of various other climate variables such as day-length, moisture, and solar radiation. Climate change can influence other environmental factors as well as early spring temperature with regard to spring phenology. For example, warmer autumns and winters can delay the dormancy onset and, in severe cases, cause trees to fail in dormancy release (Chung *et al.*, 2009). Even though changes in the local ecosystem could not be perfectly estimated, the simple

methods used in this study will be helpful to expand our understanding of the potential variation of flowering phenology related to future climate change. Further application and physiological interpretation will provide more information about possible ecosystem change in association with global warming by applying DTS or more mechanistic phenology models to many plants and regions.

Acknowledgements

This work was carried out with the support of the Korea Meteorological Administration Research and Development Program under Grant CATER 2012-3083 and the Rural Development Administration Cooperative Research Program for Agriculture Science and Technology Development under Grant Project No. PJ009953, Republic of Korea.

References

- Ahn J-B, Lee J, Im E-S. 2012. The reproducibility of surface air temperature over South Korea using dynamical downscaling and statistical correction. *J. Meteorol. Soc. Jpn.* **90**: 493–507, DOI: 10.2151/jmsj.2012-404.
- Aono Y, Kazui K. 2008. Phenological data series of cherry tree flowering in Kyoto, Japan, and its application to reconstruction of springtime temperatures since the 9th century. *Int. J. Climatol.* **28**: 905–914, DOI: 10.1002/joc.1594.
- Aono Y, Saito S. 2010. Clarifying springtime temperature reconstructions of the medieval period by gap-filling the cherry blossom phenological data series at Kyoto, Japan. *Int. J. Biometeorol.* **54**: 211–219, DOI: 10.1007/s00484-009-0272-x.
- Cannell MGR, Smith RI. 1986. Climatic warming, spring budburst and frost damage on trees. *J. Appl. Ecol.* **23**: 177–191.
- Cesaraccio C, Spano D, Snyder RL, Duce P. 2004. Chilling and forcing model to predict bud-burst of crop and forest species. *Agric. For. Meteorol.* **126**: 1–13.
- Chmielewski F-M, Blümel K, Páľešová I. 2012. Climate change and shifts in dormancy release for deciduous fruit crops in Germany. *Clim. Res.* **54**: 209–219, DOI: 10.3354/cr01115.
- Chung U, Jung J-E, Seo H-C, Yun JI. 2009. Using urban effect corrected temperature data and a tree phenology model to project geographical shift of cherry flowering date in South Korea. *Clim. Change* **93**: 447–463, DOI: 10.1007/s10584-008-9504-z.
- Chung U, Mack L, Yun JI, Kim S-H. 2011. Predicting the timing of cherry blossoms in Washington, DC and mid-Atlantic states in response to climate change. *PLoS One* **6**(11): e27439, DOI: 10.1371/journal.pone.0027439.
- Daly C, Helmer EH, Quinones M. 2003. Mapping the climate of Puerto Rico, Vieques and Culebra. *Int. J. Climatol.* **23**: 1359–1381, DOI: 10.1002/joc.937.
- Diekmann M. 1996. Relationship between flowering phenology of perennial herbs and meteorological data in deciduous forests of Sweden. *Can. J. Bot.* **74**(4): 528–537, DOI: 10.1139/b96-067.
- Dodson R, Marks D. 1997. Daily air temperature interpolated at high spatial resolution over a large mountainous region. *Clim. Res.* **8**: 1–20, DOI: 10.3354/cr008001.
- Gent PR, Danabasoglu G, Donner LJ, Holland MM, Hunke EC, Jayne SR, Lawrence DM, Neale RB, Rasch PJ, Vertenstein M, Worley PH, Yang Z-L, Zhang M. 2011. The community climate system model version 4. *J. Clim.* **24**: 4973–4991, DOI: 10.1175/2011JCLI4083.1.
- Gong D-Y, Ho C-H. 2002. The Siberian high and climate change over middle to high latitude Asia. *Theor. Appl. Climatol.* **72**: 1–9, DOI: 10.1007/s007040200008.
- Guedon Y, Legave JM. 2008. Analyzing the time-course variation of apple and pear tree dates of flowering stages in the global warming context. *Ecol. Model.* **219**: 189–199, DOI: 10.1016/j.ecolmodel.2008.08.010.
- Guo L, Dai J, Ranjekar S, Yu H, Xu J, Luedeling E. 2013. Chilling and heat requirements for flowering in temperate fruit trees. *Int. J. Biometeorol.*, DOI: 10.1007/s00484-013-0714-3.

- Hazeleger W, Severijns C, Semmler T, Ștefănescu S, Yang S, Wang X, Wyser K, Dutra E, Baldasano JM, Bintanja R, Bougeault P, Caballero R, Ekman AML, Christensen JH, Bvd H, Jimenez P, Jones C, Källberg P, Koenig T, McGrath R, Miranda P, Noije TV, Palmer T, Parodi JA, Schmith T, Selten F, Storelvmo T, Sterl A, Tapamo H, Vancoppenolle M, Viterbo P, Willén U. 2010. EC-Earth: a seamless earth system prediction approach in action. *Bull. Am. Meteorol. Soc.* **91**: 1357–1363, DOI: 10.1175/2010BAMS2877.1.
- Hur J, Ahn J-B, Shim K-M. 2014. The change of cherry first-flowering date over South Korea projected from downscaled IPCC AR5 simulation. *Int. J. Climatol.* **34**: 2308–2319, DOI: 10.1002/joc.3839.
- Im E-S, Ahn J-B. 2011. On the elevation dependency of present-day climate and future change over Korea from a high resolution regional climate simulation. *J. Meteorol. Soc. Jpn.* **89**: 89–100, DOI: 10.2151/jmsj.2011-106.
- Im E-S, Ahn J-B, Kwon W-T, Giorgi F. 2008. Multi-decadal scenario simulation over Korea using a one-way double-nested regional climate model system. Part 2: future climate projection (2021–2050). *Clim. Dyn.* **30**: 239–254, DOI: 10.1007/s00382-007-0282-5.
- Ines AVM, Hansen JW. 2006. Bias correction of daily GCM rainfall for crop simulation studies. *Agric. For. Meteorol.* **138**: 44–53, DOI: 10.1016/j.agrformet.2006.03.009.
- Intergovernmental Panel on Climate Change (IPCC). 2007. *Climate Change 2001: The Physical Science Basis. Contribution of Working Group I to the Fourth Assessment Report of the Intergovernmental Panel on Climate Change*. Solomon S, Qin D, Manning M, Chen Z, Marquis M, Averyt KB, Tignor M, Miller HL (eds). Cambridge University Press: Cambridge, UK, 1–17.
- Jeong J-H, Ho C-H, Linderholm HW, Jeong S-J, Chen D, Choi Y-S. 2011. Impact of urban warming on earlier spring flowering in Korea. *Int. J. Climatol.* **31**: 1488–1497, DOI: 10.1002/joc.2178.
- Jeong H-I, Lee DY, Ashok K, Ahn J-B, Lee J-Y, Luo J-J, Schemm J-KE, Hendon HH, Braganza K, Ham Y-G. 2012. Assessment of the APCC coupled MME suite in predicting the distinctive climate impacts of two flavors of ENSO during boreal winter. *Clim. Dyn.* **39**: 475–493, DOI: 10.1007/s00382-012-1359-3.
- Jung JE, Kwon EY, Chung U, Yun JI. 2005. Predicting cherry flowering date using a plant phenology model. *Korean J. Agric. For. Meteorol.* **7**: 148–155 (English Abstract).
- Jung M-P, Kim K-H, Lee S-G, Park H-H. 2013. Effect of climate change on the occurrence of overwintered moths of orchards in South Korea. *Entomol. Res.* **43**: 177–182, DOI: 10.1111/1748-5967.12016.
- Kim JH, Cheon JH, Yun JI. 2013. Outlook on blooming dates of spring flowers in the Korean Peninsula under the RCP8.5 projected climate. *Korean J. Agric. For. Meteorol.* **15**: 50–58 (English Abstract).
- Krishnamurti TN, Kishtawal CM, LaRow TE, Bachiochi DR, Zhang Z, Williford CE, Gadgil S, Surendran S. 1999. Improved weather and seasonal climate forecasts from multimodel superensemble. *Science* **285**: 1548–1550, DOI: 10.1126/science.285.5433.1548.
- Kwon W-T. 2005. Current status and perspectives of climate change sciences. *J. Korean Meteorol. Soc.* **41**: 325–336 (English Abstract).
- McMaster GS, Wilhelm WW. 1997. Growing degree-days: one equation, two interpretations. *Agric. For. Meteorol.* **87**: 291–399, DOI: 10.1016/S0168-1923(97).
- Menzel A, Dose V. 2005. Analysis of long-term time series of the beginning of flowering by Bayesian function estimation. *Meteorol. Z.* **14**(3): 429–434, DOI: 10.1127/0941-2948/2005/0040.
- Menzel A, Fabian P. 1999. Growing season extended in Europe. *Nature* **397**: 659, DOI: 10.1038/17709.
- Mizuta R, Yoshimura H, Murakami H, Matsueda M, Endo H, Ose T, Kamiguchi K, Hosaka M, Sugi M, Yukimoto S, Kusunoki S, Kitoh A. 2012. Climate simulations using MRI-AGCM3.2 with 20-km grid. *J. Meteorol. Soc. Jpn.* **90**: 233–258.
- Ohashi M, Tanaka HL. 2010. Data analysis of recent warming pattern in the arctic. *SOLA* **6A**: 1–4, DOI: 10.2151/sola.6A-001.
- Ono S, Konno T. 1999. Estimation of flowering date and temperature characteristics of fruit trees by DTS method. *Jpn. Agric. Res. Q.* **33**: 105–108.
- Réaumur RAF. 1735. Observations du thermomètre, faites à Paris pendant l'année 1735, comparees avec celles qui ont été faites sous la ligne, à l'Isle de France, à Alger et en quelquesunes de nos isles de l'Amérique. *Mém. Acad. R. Sci.* **1735**: 545–576.
- Roetzer T, Witzentzler M, Haeckel H, Nekovar J. 2000. Phenology in central Europe – differences and trends of spring phenophases in urban and rural areas. *Int. J. Biometeorol.* **44**: 60–66, DOI: 10.1007/s004840000062.
- Snyder RL, Spano D, Cesaraccio C, Duce P. 1999. Determining degree-day thresholds from field observations. *Int. J. Biometeorol.* **42**: 177–182.
- Taylor KE, Stouffer RJ, Meehl GA. 2012. An overview of CMIP5 and the experiment design. *Bull. Am. Meteorol. Soc.* **93**: 485–498, DOI: 10.1175/BAMS-D-11-00094.1.
- Tyler G. 2001. Relationships between climate and flowering of eight herbs in a Swedish deciduous forest. *Ann. Bot.* **87**: 623–630, DOI: 10.1006/anbo.2001.1383.
- Watanabe M, Suzuki T, O'ishi R, Komuro Y, Watanabe S, Emori S, Takemura T, Chikira M, Ogura T, Sekiguchi M, Takata K, Yamazaki D, Yokohata T, Nozawa T, Hasumi H, Tatebe H, Kimoto M. 2010. Improved climate simulation by MIROC5: mean states, variability, and climate sensitivity. *J. Clim.* **23**: 6312–6335, DOI: 10.1175/2010JCLI3679.1.
- Wielgolaski FE. 2003. Climatic factors governing plant phenological phases along a Norwegian fjord. *Int. J. Biometeorol.* **47**: 213–220, DOI: 10.1007/s00484-003-0178-y.
- Wu T, Yu R, Zhang F, Wang Z, Dong M, Wang L, Jin X, Chen D, Li L. 2010. The Beijing climate center for atmospheric general circulation model (BCC-AGCM2.0.1): description and its performance for the present-day climate. *Clim. Dyn.* **34**: 123–147, DOI: 10.1007/s00382-009-0594-8.
- Yeang H-Y. 2007. Synchronous flowering of the rubber tree (*Hevea brasiliensis*) induced by high solar radiation intensity. *New Phytol.* **175**(2): 283–289, DOI: 10.1111/j.1469-8137.2007.02089.x.
- Yukimoto S, Yoshimura H, Hosaka M, Sakami T, Tsujino H, Hirabara M, Tanaka TY, Deushi M, Obata A, Nakano H, Adachi Y, Shindo E, Yabu S, Ose T, Kitoh A. 2011. Meteorological research institute-earth system model v1 (MRI-ESM1) – model description. *Tech. Rep. Meteorol. Res. Inst.* **64**: 88.
- Yun JI, Choi J, Yoon YK, Chung U. 2000. A spatial interpolation model for daily minimum temperature over mountainous regions. *Korean J. Agric. For. Meteorol.* **2**(4): 175–182 (English Abstract).
- Yun W-T, Stefanova L, Krishnamurti TN. 2003. Improvement of the multimodel superensemble technique for seasonal forecasts. *J. Clim.* **16**: 3834–3840, DOI: 10.1175/1520-0442(2003)016<3834:IOTMST>2.0.CO;2.